American Heart Association.

Ultrastructural Changes of the Right Ventricular Myocytes in Pulmonary Arterial Hypertension

Nataliia V. Shults, MD, PhD; Sergey S. Kanovka, BS; Jennifer E. Ten Eyck, MS; Vladyslava Rybka, BA; Yuichiro J. Suzuki, PhD

Background—Pulmonary arterial hypertension (PAH) is a serious disease without cure. Elevated pulmonary vascular resistance puts strain on the right ventricle (RV) and patients die of RV failure. Subjecting Sprague–Dawley rats to SU5416 injection and hypoxia promotes severe PAH with pulmonary vascular lesions similar to human disease and has been well utilized to investigate pulmonary vascular pathology. However, despite exhibiting severe RV fibrosis, these rats do not die. Recently, subjecting Fischer (CDF) rats to the same treatment to promote PAH was found to result in mortality. Thus, the present study performed detailed morphological characterizations of Fischer rats with PAH.

Methods and Results—Rats were subjected to SU5416 injection and hypoxia for 3 weeks, followed by maintenance in normoxia. More than 90% of animals died within 6 weeks of the SU5416 injection. Necropsy revealed the accumulation of fluid in the chest cavity, right ventricular hypertrophy and dilatation, hepatomegaly, and other indications of congestive heart failure. Time course studies demonstrated the progressive thickening of pulmonary arteries with the formation of concentric lamellae and plexiform lesions as well as RV fibrosis in PAH rats. Transmission electron microscopy demonstrated the destruction of the myofilaments, T-tubules, and sarcoplasmic reticulum. RV mitochondrial damage and fission were found in Fischer rats, but not in Sprague–Dawley rats, with PAH.

Conclusions—These results suggest that the destruction of RV mitochondria plays a role in the mechanism of PAH-induced death. The SU5416/hypoxia model in Fischer rats should be useful for further investigating the mechanism of RV failure and finding effective therapeutic agents to increase the survival of PAH patients. (***J Am Heart Assoc***. 2019;8:e011227. DOI: 10.1161/JAHA.118.011227.)

Pulmonary arterial hypertension (PAH) can affect males and females of any age, including children and young adults. Despite the availability of US Food and Drug Admin- istration–approved drugs, PAH remains a fatal disease without a cure.[1,2] Increased resistance in the pulmonary artery puts strain on the right ventricle (RV), and RV failure is the major cause of death among PAH patients.[3,4] The median overall survival for patients diagnosed with PAH is 2.8 years from the time of diagnosis (3-year survival: 48%) if untreated.[5,6] Even with currently available therapies, the prognosis remains poor; only 58% to 75% of PAH patients survive for 3 years.[7–10] PAH is a progressive disease, and by the time patients are diagnosed, RV alterations have already occurred. Thus, understanding the development and progression of RV failure should help develop improved therapeutic strategies to treat PAH patients.

Since the initial discovery that treating Sprague–Dawley (SD) rats with the SU5416 injection plus chronic hypoxia promoted severe PAH with pulmonary vascular lesions that resemble those of humans,[11] this experimental model of PAH has become a criterion standard in the research field of pulmonary hypertension. The experimental design to promote PAH usually involves a single subcutaneous injection of SU5416, followed by subjecting the animals to chronic hypoxia for 3 weeks. In many published studies, rats are then maintained in normoxia for 2 to 5 weeks for studying pulmonary vascular lesions that resemble human PAH.[11–15] At this stage, some laboratories, including ours, have reported that the RV is severely damaged with fibrosis.[12,16–18] However, our laboratory found that, at 8 to 17 weeks after the SU5416 injection and the initiation of chronic hypoxia, despite the occurrence of severe fibrosis, RV contractility is

Clinical Perspective

What Is New?

- This article describes a new animal model of pulmonary arterial hypertension–induced right heart failure.
- Using transmission electron microscopy, the present study reveals the detailed ultrastructure of mitochondria in the failing right ventricle.

What Are the Clinical Implications?

- As right heart failure is the major cause of death among patients with pulmonary arterial hypertension, this model should be useful for the studies of the mechanism of right heart failure and for developing therapeutic strategies to prevent and/or treat right heart failure.

maintained or even improved because of the formation of "super" RV myocytes.[18] Moreover, our results demonstrated that, at 35 weeks after the SU5416 injection, RV fibrosis was resolved in SD rats, despite the RV pressure remaining high.[19] Thus, the SU5416/hypoxia treatment does not cause the death of SD rats.

By contrast, Fischer (CDF) rats with PAH induced by the same SU5416/hypoxia treatment were found to exhibit high mortality.[20] In the studies of Jiang et al[20] performed in Ottawa, Canada, up to 75% of Fischer rats died in the range of 3 to 8 weeks. In our laboratory in Washington, DC, this treatment resulted in >90% of rats consistently dying between 5 and 6 weeks after the initiation of the SU5416/hypoxia treatment. Since human PAH patients die of heart failure, Fischer rats treated with SU5416/hypoxia should represent an important model for the investigation of PAH. Thus, in the present study, we performed comprehensive characterizations of the Fischer rat model of PAH using histological, transmission electron microscopy (TEM), and metabolomics approaches.

Methods

The data that support the findings of this study are available from the corresponding author upon reasonable request.

Animal Treatment

Male and female Fischer (CDF) and SD (CD) rats (Charles River Laboratories International, Inc, Wilmington, MA) were randomly divided into experimental groups. Rats assigned to be in the PAH groups were subcutaneously injected with SU5416 (20 mg/kg body weight; MedChem Express, Monmouth Junction, NJ), maintained in hypoxia for up to 3 weeks[12,13,21] and then in normoxia for various durations.

Animals were subjected to hypoxia in a chamber (30 in w $\times$ 20 in d $\times$ 20 in h) regulated by an OxyCycler Oxygen Profile Controller (Model A84XOV; BioSpherix, Redfield, NY) set to maintain 10% O_2 with an influx of N_2 gas, located in the animal care facility at the Georgetown University Medical Center.[13,21] Ventilation to the outside of the chamber was adjusted to remove CO_2, such that its level did not exceed 5000 ppm. Control animals were subjected to ambient 21% O_2 (normoxia) in another chamber. Animals were fed normal rat chow. The number of experimental animals were determined by the power calculation, in which the sample size that gives an 80% chance of rejecting the hypothesis of no difference at the 0.05 levels of significance was estimated by the equation $16\sigma^2/\delta^2+1$, where δ is the difference between mean values from treated animals and untreated controls and σ is the within-group standard deviation. The Georgetown University Animal Care and Use Committee approved all animal experiments, and the investigation conformed to the National Institutes of Health (NIH) Guide for the Care and Use of Laboratory Animals.

Histological Measurements

Heart and lung tissues were immersed in buffered 10% formalin at room temperature and were embedded in paraffin. Paraffin-embedded tissues were cut and mounted on glass slides. Tissue sections were subjected to hematoxylin and eosin (H&E) stain, Verhoeff-van Gieson stain, Masson's trichrome stain, and immunohistochemistry using the α-smooth muscle actin antibody (Abcam, Cambridge, UK) or the platelet and endothelial cell adhesion molecule 1 antibody (sc-376764, Santa Cruz Biotechnology, Dallas, TX).

Transmission Electron Microscopy

RV free wall and vastus lateralis skeletal muscle tissues were fixed in the 2.5% glutaraldehyde/0.05 mol/L cacodylate solution, postfixed with 1% osmium tetroxide, and embedded in EmBed812. Ultrathin sections (70 nm) were poststained with uranyl acetate and lead citrate and examined in the Talos F200X FEG transmission electron microscope (FEI, Hillsboro, OR) at 80 kV located at the George Washington University Nanofabrication and Imaging Center. Digital electron micrographs were recorded with the TIA software (FEI).

Morphometric Analysis

Morphometric analysis was performed under blinded conditions by systematic uniform random sampling with the Fiji Software using 25 randomly selected images. The volume density of microvessels was determined by quantifying the percent areas in platelet and endothelial cell adhesion molecule 1 immunostained slides. The microvessels were

defined as round or ellipse structures with a central lumen lined by endothelial cells staining positively to platelet and endothelial cell adhesion molecule 1 antibody with diameters >20 mm and <100 mm. In TEM images, the number, area (S), and volume density[22,23] of organelles were determined using the morphometric technique with a dot grid.[24] Mitochondrial types, mitochondria clusters, and intermitochondrial junctions (IMJ) were determined using the point counting method.[25] The coefficient of energy efficiency of mitochondria (CEEM) was defined as the product of the number of mitochondrial cristae and the area of mitochondria.[26]

Metabolomics

RV tissues were homogenized in 50% methanol containing internal standards and then centrifuged for 10 minutes. An equal volume of chilled acetonitrile was added to each sample tube, and then vortexed and incubated overnight at −20°C. Tubes were again centrifuged for 10 minutes at room temperature, and the supernatant was transferred to fresh tubes and dried under vacuum. The dried metabolite mixture was resuspended in 100 µL of 50% methanol for mass spectrometry analysis. Samples were injected onto a reverse-phase column using an Acquity ultraperformance liquid chromatography system (Waters Corporation, Milford, MA). Mass spectrometry was performed by using a quadrupole-time-of-flight mass spectrometer operating in either negative or positive electrospray ionization mode with a capillary voltage of 3.2 kV and a sampling cone voltage of 35 V. Data were acquired in centroid mode with a mass range from 50 to 850 m/z for time-of-flight mass spectrometry scanning.[19,27]

Statistical Analysis

Means and standard errors were calculated. Comparisons between 2 groups were analyzed by using a 2-tailed Student *t* test and comparisons between 3 or more groups were analyzed by using 1-way ANOVA with a Student-Newman-Keuls post-hoc test using the GraphPad Prism (GraphPad Software, Inc, La Jolla, CA).[13] $P<0.05$ was considered to be significant. The Kaplan–Meier survival curve was used as previously described.[28]

Results

Fischer Rats Treated With SU5416/Hypoxia Die of Congestive Heart Failure

Fischer (CDF) rats were injected with SU5416, placed in hypoxia for 3 weeks, and then maintained in normoxia. In our experiments, conducted in our laboratory in Washington, DC, 93.7% of PAH rats died within 6 weeks of the SU5416

injection (N=16) (Figure 1A). PAH rats lost some weight during the first week after the SU5416 injection, but subsequently the rate of weight gain by PAH rats was comparable with that of control rats (Figure 1B). Necropsy of PAH rats that died consistently showed hydrothorax (with the mean fluid volume in the chest cavity being ≈6 mL), mild ascites, and anasarca. The lung surface was heterogeneous with an excessive airiness. The pathological examination of the heart showed an enlargement on both the left and right sides of the heart, resembling "cor pulmonale." Cross-sections of the heart revealed eccentric hypertrophy with ventricular wall thickening and dilated ventricular cavities as shown in Figure 1C. Both RV and left ventricle (LV) of PAH rats exhibited increased wall thickness. Fulton index RV/(LV+S), an indicator of RV hypertrophy, doubled in PAH rats compared with controls (Table). Indications of right heart failure in PAH rats also included hepatomegaly (11.9 g in PAH rats versus 8.9 g in controls), "nutmeg liver," splenomegaly (0.9 g in PAH rats versus 0.5 g in controls), and the cyanotic induration of the spleen and kidney.

Histological examinations of postmortem RV tissues of PAH rats stained with H&E revealed polymorphic changes in cardiomyocytes, hypereosinophilia with contraction bands (arrow), the hypertrophy and atrophy of cardiomyocytes, and the rearrangement and focal lysis of myofibers (arrowhead) (Figure 1D). H&E staining of the postmortem liver of PAH rats showed that the central vein and sinusoids of centrilobular regions were distended and the portal tracts were congested (Figure 1E). Hepatocytes of postmortem PAH rats exhibited atrophy and hemorrhagic necrosis along with a fatty change in the central zone and a swelling in the peripheral zone.

Pulmonary Vascular Remodeling in Fischer Rats With PAH

To examine the progression of pulmonary vascular changes, Fischer rats were injected with SU5416, placed in hypoxia for up to 3 weeks, and then maintained in normoxia for up to 2 weeks to obtain time points of 0, 1, 2, 3, 4, and 5 weeks after the SU5416 injection. Rats were then euthanized and histological data were obtained. H&E staining revealed progressive alterations in the lung structure including alveolar wall thickening, emphysematous hyperdistention of alveolar ducts, and remodeling of pulmonary vessels (Figure 2A). Pulmonary arteries (PAs) showed pathological features including medial hypertrophy, intimal proliferation, concentric lamellar fibrosis, and plexiform lesions in PAH rats. H&E staining demonstrated the presence of intimal endothelial cell proliferation, increased PA wall thickness, and the reduction of the lumen that occurs as early as 1 week after the SU5416 injection (Figure 2B). At 4 to 5 weeks after the SU5416
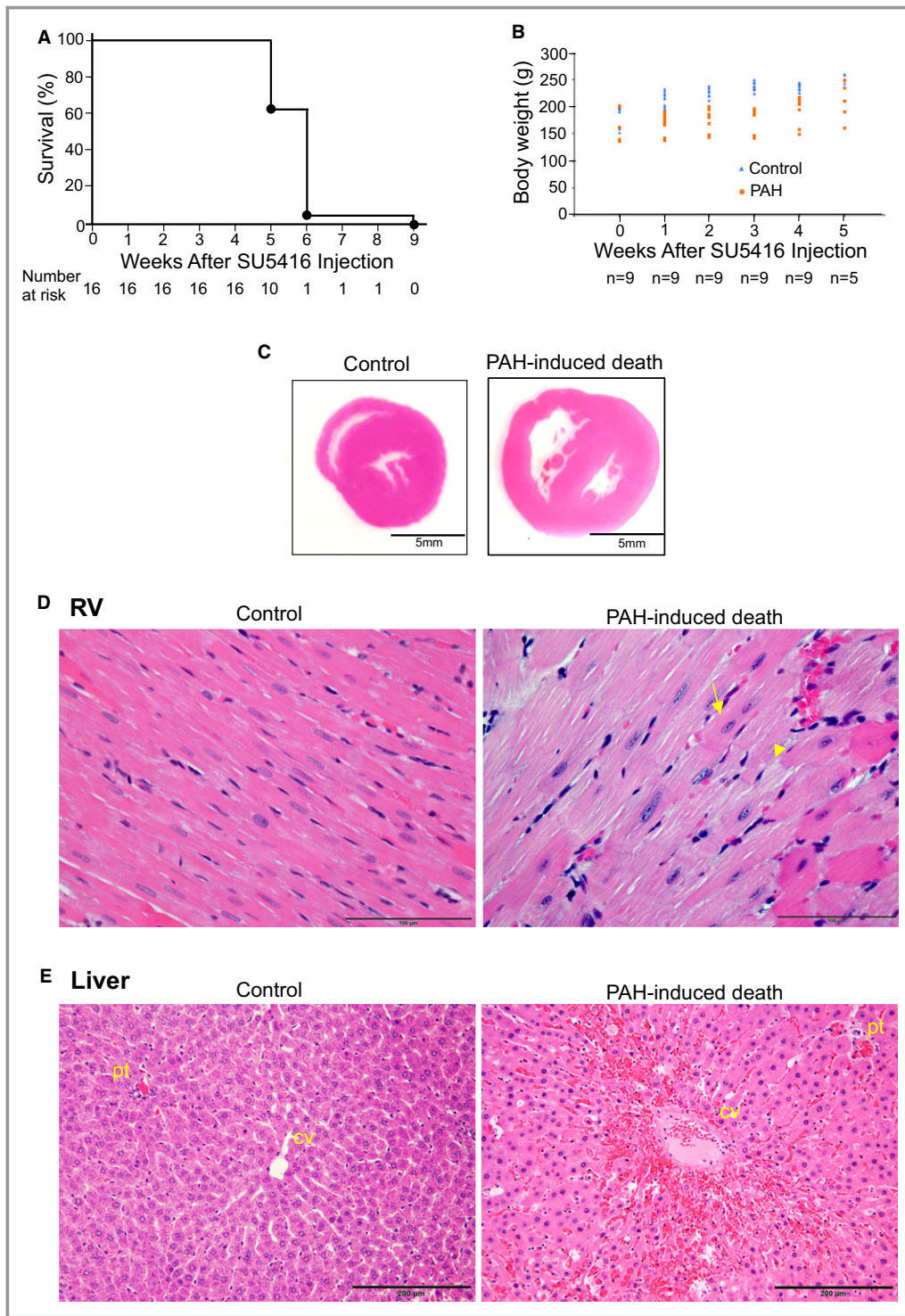
Figure 1. SU5416/hypoxia-treatment of Fischer rats results in congestive heart failure and death. Fischer (CDF) rats were injected with SU5416, placed in hypoxia for 3 weeks, and subsequently maintained in normoxia to produce PAH. **A**, Kaplan–Meier survival curve of rats treated with SU5416/hypoxia. **B**, Scatter graph showing the body weight in grams (g). **C**, Representative cross-sections of the whole heart in control and rats that died of SU5416/hypoxia. Scale bars, 5 mm. **D**, Representative H&E stain images of the RV of control and rats that died of SU5416/hypoxia. Magnification ×400. **E**, Representative H&E stain images of the liver of control and rats that died of SU5416/hypoxia. Magnification ×200. Cv indicates central vein; H&E, hematoxylin and eosin; PAH, pulmonary arterial hypertension; pt, portal tracts; RV, right ventricle.

Table. Characteristics of Fischer Rats With PAH in Response to SU5416/Hypoxia (5 Weeks After SU5416 Injection)

n=12	Control	PAH
BW, g	252.9±4.1	201.3±11.3*
Heart, g	0.811±0.020	1.053±0.045*
RV, mg	15.0±0.9	32.7±1.9*
RV/BW, mg/g	0.06±0.004	0.17±0.013*
LV+S, mg	58.8±1.1	60.0±4.0
LV+S/BW, mg/g	0.23±0.004	0.30±0.01*
RV/(LV+S)	0.26±0.02	0.57±0.05*
Lung, g	1.6±0.19	1.5±0.04
Tibia, cm	4.8±0.2	4.6±0.2

BW indicates body weight; LV, left ventricular weight; LV+S, left ventricular weight plus septal weight; n, number of rats; PAH, pulmonary arterial hypertension; RV, right ventricular weight. Values represent means±SEM.
*Significantly different from control at $P<0.05$.

injection, many of the PAs were found to be completely occluded with the indication of plexiform lesions (Figure 2C, arrow). Quantifications of the H&E staining images indicated the progressive wall thickening (Figure 2D) and occlusion (Figure 2E) of small PAs (30−100 μm in diameter).

Figure 2F shows the various histological characteristics of the PAs of PAH rats at 5 weeks after the SU5416 injection and controls. The Verhoeff-van Gieson stain showed the shirring of the internal elastic membrane, the destruction of the external elastic membrane in the PA, and increased elastic fibers in the medial layer. Masson's trichrome stain demonstrated excess collagen fibers in the media and adventitial layers in the PAs of PAH rats. Immunohistochemistry indicated increased α-smooth muscle actin expression in the PAs of PAH rats.

Hypertrophy and Fibrosis

The H&E staining of the heart showed progressive RV wall hypertrophy and cavity enlargement in response to SU5416/hypoxia (Figure 3A). The cross-section of the H&E-stained micrographs of the RV myocardium demonstrated progressive cardiomyocyte hypertrophy in PAH rats (Figure 3B). Figure 3E presents the quantification of the diameters of RV myocytes at various time points after the SU5416 injection. The longitudinal section of the RV myocardium indicated polymorphic changes in RV myocardium (Figure 3C). The initial alterations of the RV myocardium were present at 1 week after the SU5416 injection including the disorientation of myofibers, interstitial edema, and uneven hypertrophy of cardiomyocytes along with the deformation of the nuclei in sizes and shapes. Dystrophic alterations of hypertrophied RV cardiomyocytes were initiated at 1 to 2 weeks after the

SU5416 injection manifested in focal eosinophilia cardiomyocytes. At 3 to 4 weeks, the hypertrophy and atrophy of cardiomyocytes had become pronounced, the wavy arrangement of myofibers (3 weeks, arrowhead) was observed along with the contractures of cardiomyocytes (3 weeks, arrow) and loci with the focal lysis of cardiomyocytes (4 weeks, arrows). Evidence of myofiber disarray (5 weeks, arrowhead) and focal myocytolysis (5 weeks, arrow) was also obtained (Figure 3C).

Masson's trichrome staining of the RV myocardium of Fischer rats treated with SU5416/hypoxia showed progressively increased interstitial fibrosis and an appearance of the loci of replacement-type fibrosis (Figure 3D). At 1 to 2 weeks after the SU5416 injection, the amount of fibrosis tissue increased by 1–2%, perhaps because of interstitial-type fibrosis. At 3 to 5 weeks after the SU5416 injection, the foci of replacement-type fibrosis, as a potentially reparative reaction to the lysis of the cardiomyocytes, were observed. At 5 weeks after the SU5416 injection, the percentage of fibrotic tissues increased to 8% (Figure 3F). By contrast to a dramatic occurrence of fibrosis in the RV, the occurrence of fibrosis was minimal in the LV (Figure 3G).

Immunohistochemistry staining with an endothelial marker platelet and endothelial cell adhesion molecule 1 was used to determine the microvessels in the RV myocardium. We found that the microvessel density in the RV of Fischer rats with PAH (2.6±0.5%) was significantly lower than that in control rats (5.9±0.2%).

TEM Studies of the Contractile Apparatus of RV Cardiomyocytes

The TEM analysis of the RV myocardium of control Fischer rats indicated normal cytoarchitectonic structures of cardiomyocytes with continuous, regularly spaced myofibrils alternating with serially arranged and elongated mitochondria (Figure 4A). The morphometric analysis determined that the mean lengths of the RV sarcomere are 1.78 μm during stretch, 1.14 μm at rest, and 0.52 μm during shortening in control rats. The mean length of myosin filaments is 1.65 μm and the thickness is 10 nm. The length of the actin filament ranges from 0.7 to 0.9 μm with the mean thickness of 6 nm. The mean volume density of myofibrils is 52.6% of the total cardiomyocyte volume (Figure 4G).

By contrast, the RV cardiomyocytes of PAH rats treated with SU5416/hypoxia for 5 weeks exhibited the disruption of cytoarchitectonic structures. The sarcomere structure was destroyed, and Z-lines were mismatched, blurred, and in some areas absent (Figure 4C, arrow). In the PAH RV, I-bands and A-bands were no longer well defined. In many of these RV cardiomyocytes, myofilaments were present in different orientations (Figure 4C). The data also show the destruction
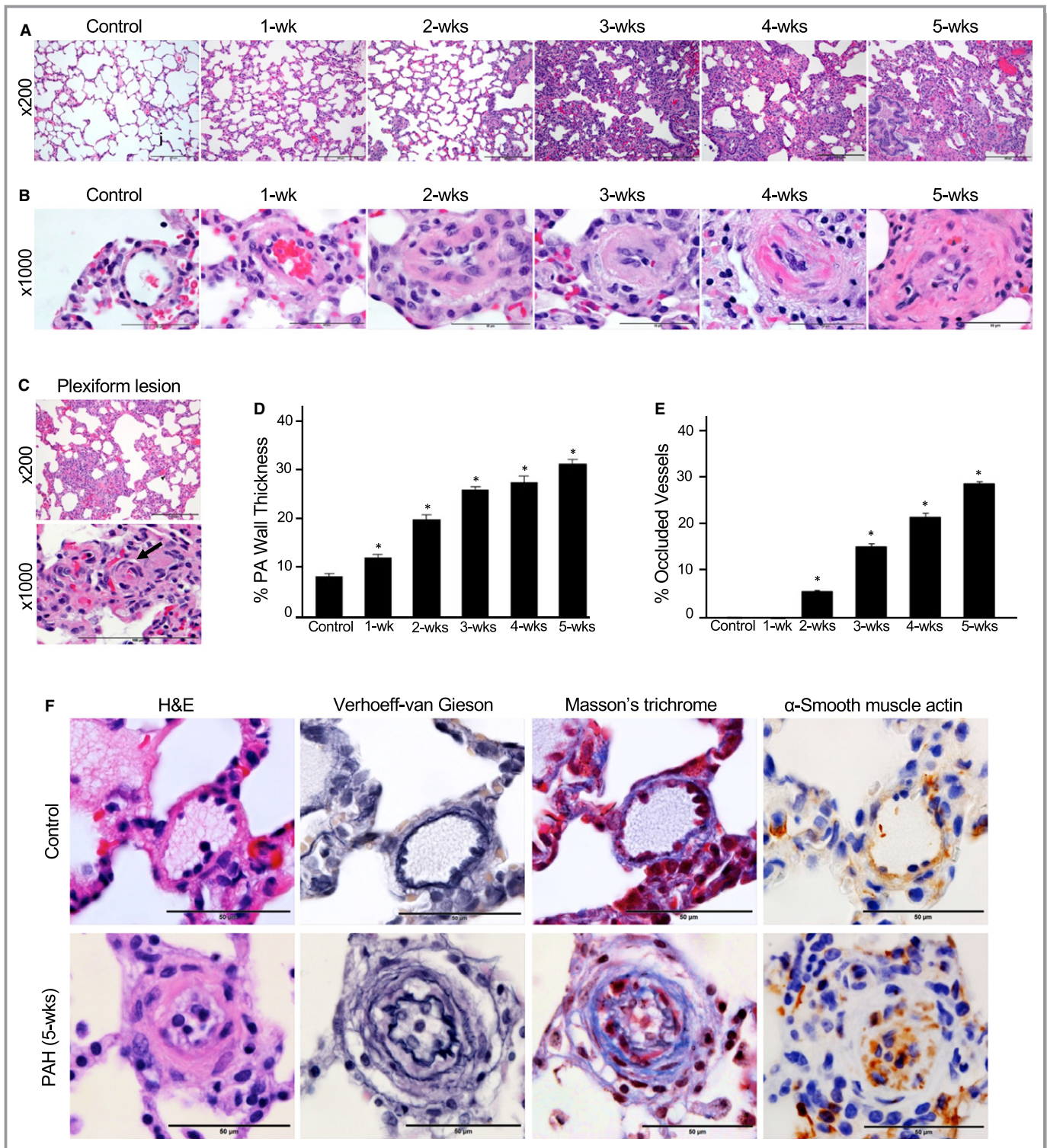
Figure 2. Histological examinations of the lung of Fischer rats treated with SU5416/hypoxia. Fischer (CDF) rats were injected with SU5416, placed in hypoxia for 3 weeks and subsequently maintained in normoxia for up to 2 weeks to promote PAH. Rats were then euthanized at various durations after the SU5416 injection. **A,** Hematoxylin and eosin (H&E)-stained lungs at ×200 magnification. **B,** H&E-stained lungs at ×1000 magnification showing small pulmonary arteries. **C,** H&E staining showing the occurrence of plexiform lesions in rats treated with SU5416/hypoxia. **D,** The bar graph represents means±SEM of % PA wall thickness. **E,** The bar graph represents means±SEM of %-occluded PAs (30–100-μm diameter). *Significantly different from control at $P<0.05$. **F,** H&E staining, Verhoeff-van Gieson staining, Masson's trichrome staining, and immunohistochemistry detecting α-smooth muscle actin of PA from control and PAH rats. Magnification ×1000. H&E indicates hematoxylin and eosin; PA, pulmonary artery; PAH, pulmonary arterial hypertension.
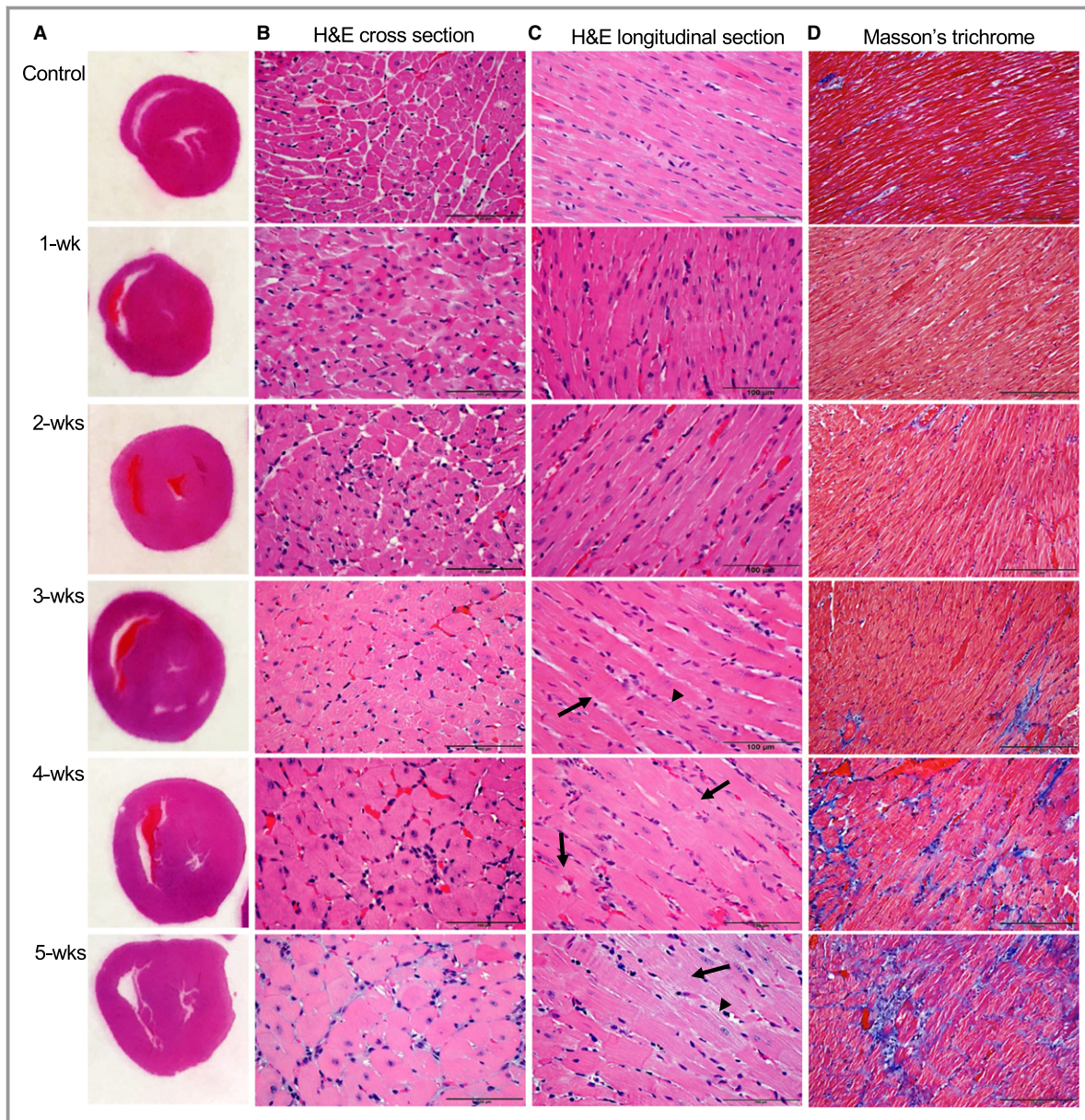
Figure 3. Histological examinations of the heart of Fischer rats treated with SU5416/hypoxia. Fischer (CDF) rats were injected with SU5416, placed in hypoxia for 3 weeks, and subsequently maintained in normoxia for up to 2 weeks. Rats were then euthanized at various durations after the SU5416 injection. **A**, H&E-stained whole-heart cross-sections. **B**, H&E-stained cross-sections of the RV myocardium. Magnification ×400. **C**, H&E-stained longitudinal-section of the RV myocardium. Magnification ×400. **D**, Masson's trichrome staining of longitudinal-section of the RV myocardium showing fibrosis tissues (blue stains). Magnification ×400. **E**, The bar graph represents means±SEM of single cardiomyocyte thickness. **F**, The bar graph represents means±SEM of % fibrotic area as determined by analyzing the Masson's trichrome staining. *Significantly different from control at $P<0.05$. **G**, Masson's trichrome staining of longitudinal-section of the LV myocardium. Magnification ×400. H&E indicates hematoxylin and eosin; LV, left ventricle; RV, right ventricle.

of the contractile filaments system such as "mosaic melting" (Figure 4E, arrow) and diffuse and focal lysis (Figure 4E, arrowhead). The sarcomere length varies from 1.3 to 1.7 μm at 1 week and 0.8 to 1.9 μm at 5 weeks after the SU5416 injection at rest, because of the reduction in the I-band length. The volume density of myofilaments was found to be significantly increased at 1 week after the SU5416 injection (Figure 4G), consistent with the occurrence of compensatory hypertrophy. At 5 weeks after the SU5416 injection, the volume density of the myofilaments was subsequently reduced, perhaps because of the progressive lysis of the contractile apparatus (Figure 4G).
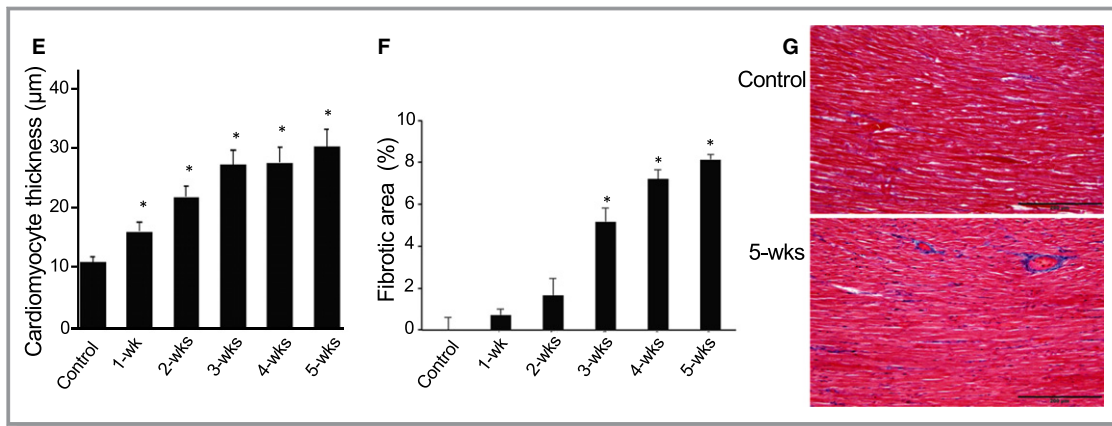
Figure 3. (Continued)

TEM Studies of the Sarcolemma of RV Cardiomyocytes

The TEM results also show that the sarcolemma of the RV cardiomyocytes of control rats has the usual contours with an evenly distributed electron-lucent glycocalyx, which is 40 to 50 nm thick (Figure 4B, arrow). The large invaginations of the sarcolemma/T-tubule range from 50 to 200 nm in diameter and contain an electron-dense material that is consistent with the normal sarcolemma. The T-system is largely coupled with the sarcoplasmic reticulum (SR) with an electron-dense space of 9 to 10 nm, forming dyads or triads, where T-tubules are flattened and their lumen has an electron-dense content (Figure 4A, arrow). The mean volume density of the T-tubules of the RV of control rats is 15% (Figure 4H). The small invaginations of the sarcolemma (caveolae and coated vesicles) range from 50 to 70 nm in diameter and contain a low electron density material (Figure 4B, arrow).

In PAH rats, the sarcolemmal contour at 5 weeks after the SU5416 injection was vague with electron-dense loci (Figure 4D, arrow). The detachment of the sarcolemma from Z-lines forced by a subsarcolemmal edema was observed (Figure 4D). The distribution of the glycocalyx layer on the sarcolemmal surface was uneven and varied in thickness (60–170 nm). The caveolae of the sarcolemmal surface in PAH rats were increased in number and size (diameter 80–100 nm) compared with controls (Figure 4D). The RV cardiomyocytes of PAH rats exhibited expanded T-tubules (250–300 nm in diameter) with high current electron-dense materials (Figure 4F, arrow). The volume density of the T-tubule was, however, reduced at 1 and 5 weeks after the SU5416 injection compared with controls (Figure 4H).

TEM Studies of the SR of RV Cardiomyocytes

The SR of control Fischer rats ranges from 15 to 40 nm in diameter with a mean wall thickness of 6 nm. TEM showed 2

types of SRs: transversely oriented tubules with an electron-lucent material that formed a network of tubules at M-line and Z-line sites united by numerous longitudinally oriented tubules and terminal cisternae that form dyads and triads with T-tubules. The mean volume density of the SR in the RV cardiomyocytes of control rats was determined to be 21.6% (Figure 4I).

The TEM examination revealed the reorganization and an uneven expansion of the SR at 5 weeks after the SU5416 injection (Figure 4F). In the Z-line regions, the SR of the PAH rats is expanded to 250 to 300 nm in diameter at 5 weeks after the SU5416 injection. The contour of the SR membrane was found to be cogged with the loci of defects and fragmentations. The coupling of the SR and T-tubule was disrupted in PAH rats (Figure 4F). The volume density of the SR was progressively reduced at 1 and 5 weeks after the SU5416 injection (Figure 4I).

TEM Studies of the Mitochondria Structure in RV Cardiomyocytes

TEM images of the RV of rats treated with SU5416/hypoxia for 5 weeks show a disruption of the mitochondrial distribution and polymorphism of the mitochondrial ultrastructure (Figure 5A). We established that after 1 week of the SU5416 injection, the disruption of the orderly chain-like structure of the mitochondria occurred only in some cardiomyocytes. After 5 weeks of the SU5416 injection, mitochondria were chaotically located in all areas of the cardiomyocyte (Figure 5A). The morphometric analysis revealed the increased number of mitochondria (20.3 ± 0.3 mitochondria per field in control versus 36.2 ± 0.2 in 5 weeks PAH) as well as mitochondrial clusters in RV cardiomyocytes with a reduction in the number of mitochondria per cluster at 1 week after the SU5416 injection. At 5 weeks, the number of mitochondrial clusters increased significantly because of mitochondrial disunion and the reduction in mitochondrial numbers per
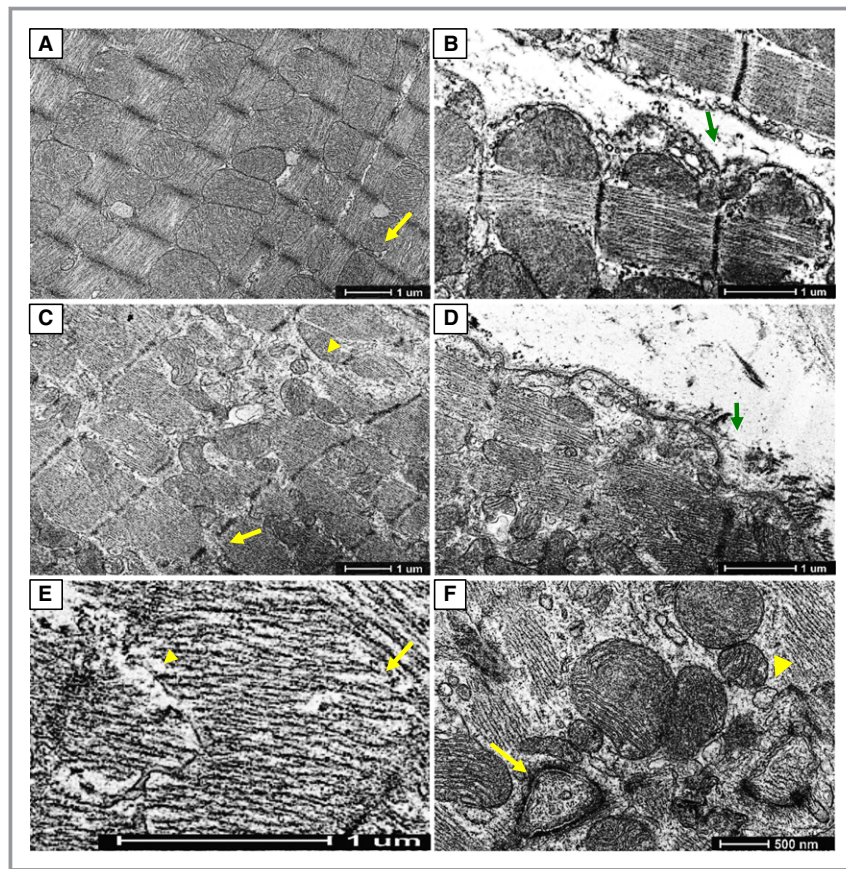
Figure 4. TEM analysis of RV cardiomyocytes of control rats and rats treated with SU5416/hypoxia. Fischer (CDF) rats were injected with SU5416, placed in hypoxia for 3 weeks and subsequently maintained in normoxia for 2 weeks to promote PAH. Rats were euthanized 1 week or 5 weeks after the SU5416 injection. **A,** A representative TEM image of the RVs of control rats demonstrating the normal cardiomyocyte cytoarchitectonic structure with continuous, regularly spaced myofibrils alternating with serially arranged and elongated mitochondria. The arrow indicates the triad. I-bands are bisected by the Z-line and A-bands show a less dense zone in the center; H-zones are bisected by the M-line. Magnification ×5500. **B,** A representative TEM image of the RVs of control rats demonstrating the small invaginations of the sarcolemma—caveolae and coated vesicles (arrow). Magnification ×11 000. **C,** A representative TEM image of the RVs of PAH rats (5-week time point) showing the disruption of normal cardiomyocyte cytoarchitecture. Discrepancies between the sarcomeres and the mismatching of the sarcomere structure with blurred and/or an abject lack of Z-lines are present (arrow). The compositions of I- and A-bands are destroyed. Different orientations of the myofilaments and diffuse and/or focal lysis are present (arrowhead). Magnification ×5500. **D,** A representative TEM image of the RVs of PAH rats (5-week time point) showing the vague contour of the sarcolemma with electron-dense loci. The glycocalix is thickened with uneven distribution (arrow). The number and size of pinocytotic vesicles are increased. Magnification ×11 000. **E,** A representative TEM image of the RVs of PAH rats (5-week time point) showing degenerative ultrastructural changes of cardiomyocyte including mosaic melting (arrow), diffuse and focal lysis of myofilaments (arrowhead). Magnification ×65 000. **F,** A representative TEM image of the RVs of PAH rats (5-week time point) showing the reorganization and expansion of T-tubule and the SR. T-tubules contain high electron density materials (arrow). The membrane of the SR is cogged with loci of defects and fragmentations (arrowhead). Magnification ×13 000. **G,** Means±SEM of % volume density of myofibrils in controls and rats with PAH (1- and 5-week time points). **H,** Means±SEM of % volume density of T-tubule in controls and rats with PAH (1- and 5-week time points). **I,** Means±SEM of % volume density of the SR in controls and rats with PAH (1- and 5-week time points). *Significantly different from each other at $P<0.05$. PAH indicates pulmonary arterial hypertension; RV, right ventricle; SR, sarcoplasmic reticulum; TEM, transmission electron tomography.
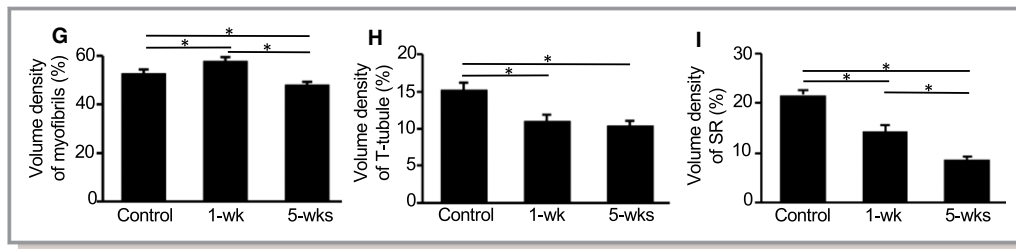
Figure 4. (Continued)

cluster (Figure 5D). One week after the SU5416 injection, the mitochondria increased in size and number. However, at 5 weeks, the size of mitochondria dramatically reduced (Figure 5C), and degenerative changes of this organelle were observed (Figure 5A). The morphometric analysis revealed that the mean percentage of the mitochondrial area in the RV cardiomyocytes of control rats is 37.6% (Figure 5B). The percentage of the mitochondrial area in cardiomyocytes increased at 1 week, but reduced at 5 weeks after the SU5416 injection (Figure 5B).

The TEM analysis of vastus lateralis skeletal muscle cells from Fischer rats after 5 weeks of SU5416/hypoxia treatment also revealed the disruption of contractile elements with multifocal lysis of myofibrils and severe mitochondrial degenerative changes compared with the normal ultrastructure in control rats (Figure 5E). The mitochondrial inner membrane is destroyed completely into the swollen matrix in most of muscle cells. Under a higher magnification as shown in Figure 5F, the edema (arrow) and the cristae fragmentation (arrowhead) were clearly observed in the skeletal muscle cells of Fischer rats with PAH.

Electron micrographs showed evenly distributed mitochondria in all regions of the cardiomyocyte (subsarcolemmal, intermyofibrillar, and perinuclear) in control rats. Mitochondria are usually oval in shape and 0.7 to 1 μm in size, containing transversally oriented cristae within a moderately electron-dense mitochondrial matrix (Figure 5A). Layers of mitochondria are located along myofibrils and tightly connected with dyads or triads in Z-line regions (Figure 5A, arrow). In these layers, mitochondria are connected by contact structures and form chain-like structures, assembled to numerous clusters. Under low magnification, contact structures look like electron-dense lines between neighboring mitochondria, namely, IMJ.[29,30] The examination of high magnification TEM images (Figure 6A) revealed that this is a uniquely organized intermembrane contact structure with characteristic morphological signs: a compact border, the confluence of the outer mitochondrial membranes of contacting mitochondria, a significant increase in the electron density of the outer and inner mitochondrial membranes, and the condensation of an electron-dense substance of the intermembrane space in the contact zone. We define that this is a limited area (loci) of

specific electron-dense IMJ (EDIMJ).[29] Figure 6A presents EDIMJ as a limited area (loci) joining the external membranes of the adjoining mitochondria. These areas are formed by an increased electron density of the contacting mitochondrial membranes and the condensation of an electron-dense substance of the intermembrane space (Figure 6A, arrows). The morphometric analysis revealed that the mean percentage of EDIMJ is 36.3% of the total IMJ in the RV of control rats (Figs. 6D and 6E).

The electron microphotographs show the merger of outer mitochondrial membranes along with the increased loci of EDIMJ in the RV cardiomyocytes of PAH rats at 1 week (Figure 6B, arrow). The mean percentage of EDIMJ was determined to be 43.4% (Figure 6E), perhaps making it possible to preserve the electrochemical potential for ATP synthesis in damaged mitochondria and allow the even distribution of energy to myofibrils. Five weeks after the SU5416 injection, the mean percentage of total IMJ significantly increased to 45% (Figure 6D), but the amount of EDIMJ reduced (Figure 6E). EDIMJ were present as a complete merger of outer mitochondrial membranes, which look like a condensation of the electron-dense substance (Figure 6C, arrow).

Through the TEM analysis, the progressive alteration of the mitochondrial structure was also evident in rats treated with SU5416/hypoxia for 5 weeks. Based on the type of mitochondrial restructuring, 4 categories were assigned (I-IV) (Figure 7A). Type I is the oval-shaped mitochondria with longitudinally oriented and tightly packed cristae. IMJ with electron-dense loci are formed between these mitochondria. Type II is the abnormal mitochondria with a nondistinct shape and/or nonuniform size with signs of hypoplasia. The cristae are swollen and/or have signs of homogenization, irregular or whirling, which usually have lost the longitudinal orientation, tightness, regular spacing, and electron-lucent matrix. Type III is the mitochondria with hypoplasia and degenerative changes. The shape and size of these mitochondria varied with a discontinuous outer membrane. The focal disruption of the inner membrane leads to an uneven increase in the crista thickness, homogenization and fragmentation, with a swollen electron-lucent matrix. Type IV is the mitochondria with disrupted and discontinuous outer membranes, deficient in
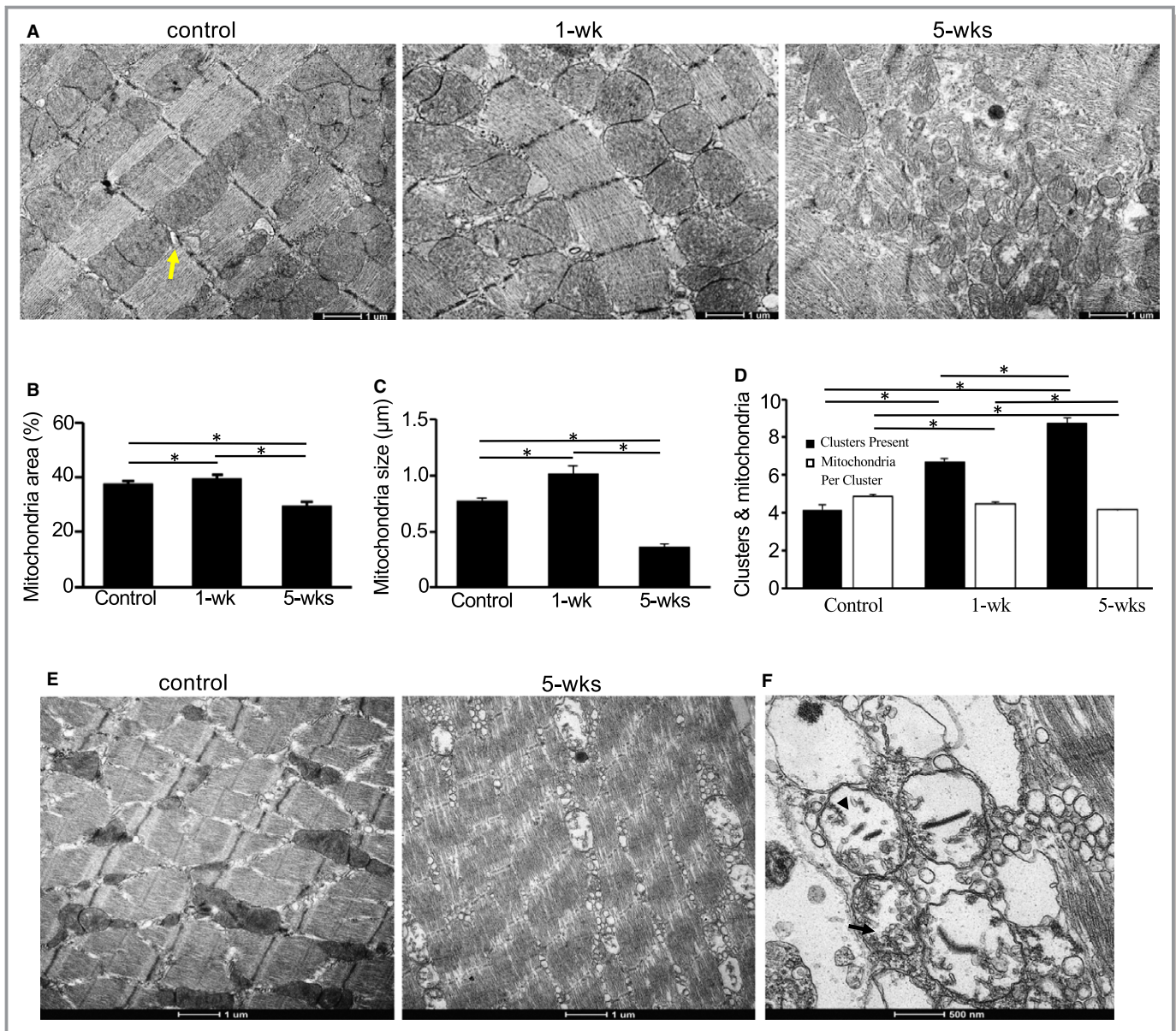
Figure 5. TEM analysis of RV cardiomyocyte mitochondria of control rats and rats treated with SU5416/hypoxia. Fischer (CDF) rats were injected with SU5416, placed in hypoxia for 3 weeks, and subsequently maintained in normoxia for 2 weeks to promote PAH. Rats were euthanized 1 week or 5 weeks after the SU5416 injection. **A**, The representative TEM image from control rats showing even distributions of the mitochondria in the RV cardiomyocyte. The chain-like structure of the mitochondria is assembled to clusters along myofibrils and tightly connected with triad in the Z-line region (arrow). At 1 week, the initial disunion of the mitochondrial clusters and the disruption of the orderly chain-like structure were visible. At 5 weeks, the disruption of mitochondrial clusters and significant polymorphism of the mitochondrial ultrastructure were observed. Magnification ×5500. **B**, Means±SEM of % of the mitochondrial area. **C**, Means±SEM of mitochondrial size. **D**, Means±SEM of mitochondrial clusters in cardiomyocyte and the number of mitochondria per cluster. *Significantly different from each other at $P<0.05$. **E**, TEM images of the vastus lateralis skeletal muscle from PAH rats showing the disruption of myofibrillar and mitochondrial structures in contrast to the well-organized normal skeletal muscle structure in control. Magnification ×5500. These differences were replicated in 3 control and 3 PAH rats. **F**, Features of mitochondrial cristae edema; fragmentation and homogenization are visible in the vastus lateralis muscle from PAH rats. Magnification ×11 000. PAH indicates pulmonary arterial hypertension; RV, right ventricle; TEM, transmission electron tomography.

cristae and "myelin-like" transformations. Initial changes to the mitochondrial structure occur as early as 1 week after the SU5416 injection, when the presence of Type II mitochondria becomes evident (Figure 7B). Substantial portions of

mitochondria in the RV cardiomyocytes at 5 weeks after the SU5416 injection were found to be Type III and Type IV (Figure 7B). By contrast, the RV cardiomyocytes of SD rats largely contained Type I and Type II mitochondria and the
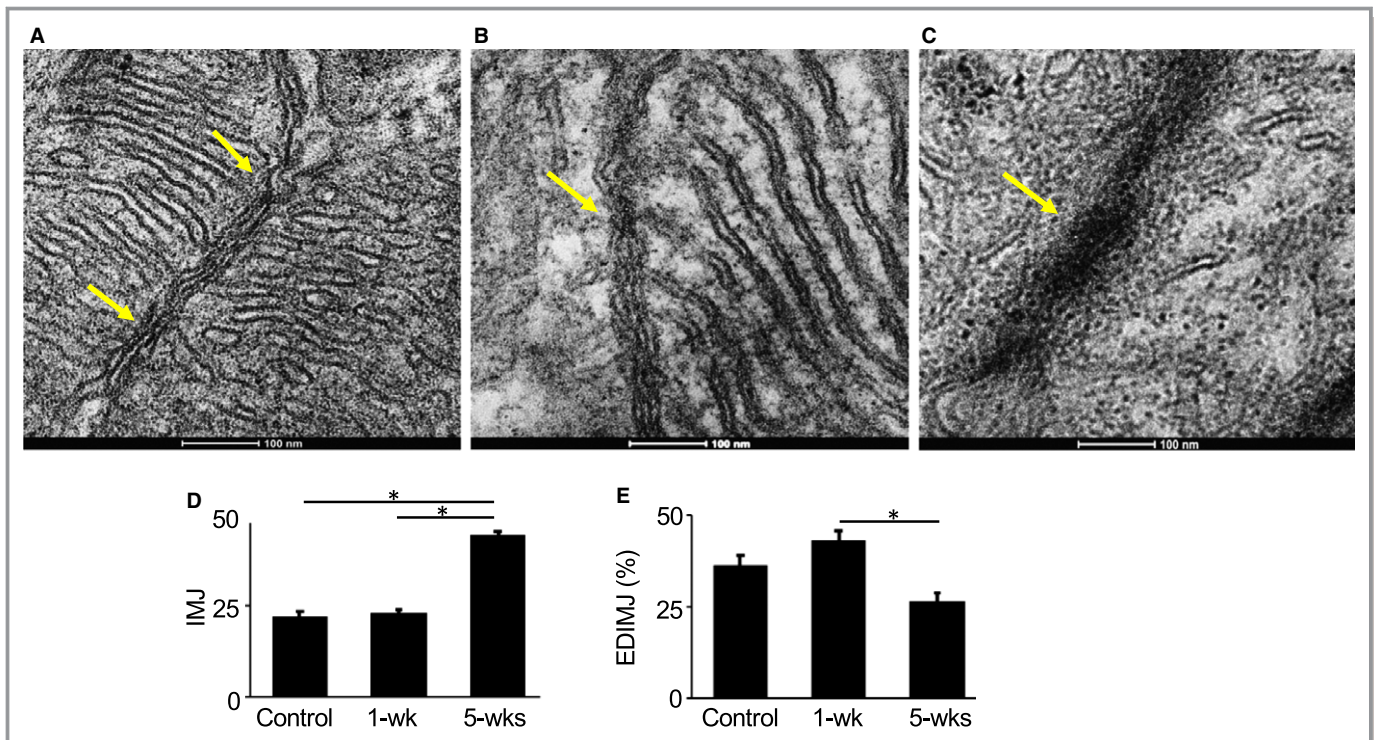
Figure 6. TEM analysis of IMJ and EDIMJ. **A**, A representative TEM image of control rats showing morphological signs of IMJ: a compact border, the confluence of the outer mitochondrial membranes with significant increase in the electron density of the outer and inner mitochondrial membranes (EDIMJ, arrows). Magnification ×120 000. **B**, The merger of outer mitochondrial membranes with a condensation of electron-dense substance of the intermembrane space in the contact zone (EDIM, arrows). Magnification ×120 000. **C**, The complete merger of outer mitochondrial membranes of destructed mitochondria with the formation EDIMJs (arrow). Magnification ×120 000. **D**, Means±SEM of IMJ. **E**, Means±SEM of % of EDIMJ. *Significantly different from each other at $P<0.05$. EDIMJ indicates electron-dense intermitochondrial junctions; IMJ, intermitochondrial junctions; TEM, transmission electron tomography.

presence of Type III and Type IV was negligible at 17 weeks after the initiation of SU5416/hypoxia treatment (Figure 7C) when severe RV fibrosis occurs.[18,19] Similarly, neither Type III nor IV mitochondria were observed in the LV of Fischer rats treated with SU5416/hypoxia.

The CEEM has been reported to estimate energy production.[26] The mitochondrial area and number of cristae were measured and the CEEM was calculated as the product of the number of cristae and area of mitochondria. The mean CEEM was found to be reduced by 30.6% at 1 week after the SU5416 injection and by 68.1% at 5 weeks (Figure 7D).

Metabolomics

Metabolomics analysis was performed to identify metabolites that are differentially expressed in the RV of PAH rats (5 weeks after the SU5416 injection) and controls. We found that oxidized glutathione was 2.3 times higher in the RV of PAH rats ($P=0.0372$), indicating the occurrence of oxidative stress. Some of the molecules that participate in energy metabolism were found to be higher in the RV of PAH rats than in controls: acetylcarnitine (3.8-fold, $P=0.0017$),

acetyl-CoA (2.5-fold, $P=0.0242$), and flavin adenine dinucleotide (3.0-fold, $P=0.0185$).

Discussion

In the present study, using a rat model of PAH that more closely resembles human disease and exhibits congestive heart failure–mediated death, we obtained critical information on the ultrastructural changes. Since PAH patients are often diagnosed after developing significant RV alterations and RV failure is the major cause of death among these patients,[3,4] therapeutic strategies to prevent and/or treat RV dysfunctions would have a tremendous impact on reducing mortality and mobility. Detailed morphometric information that was obtained for the first time in the situation of PAH-induced death should help achieve this goal.

Jiang et al[20] tested several rat strains for their responsiveness to SU5416/hypoxia and found that the Fischer (CDF) rat strain exhibits the mortality. The authors reported that the SU5416/hypoxia treatment, which increased systolic RV pressure to 100 mm Hg, caused up to 75% of Fischer rats to die 3 to 8 weeks after the SU5416 injection. In our
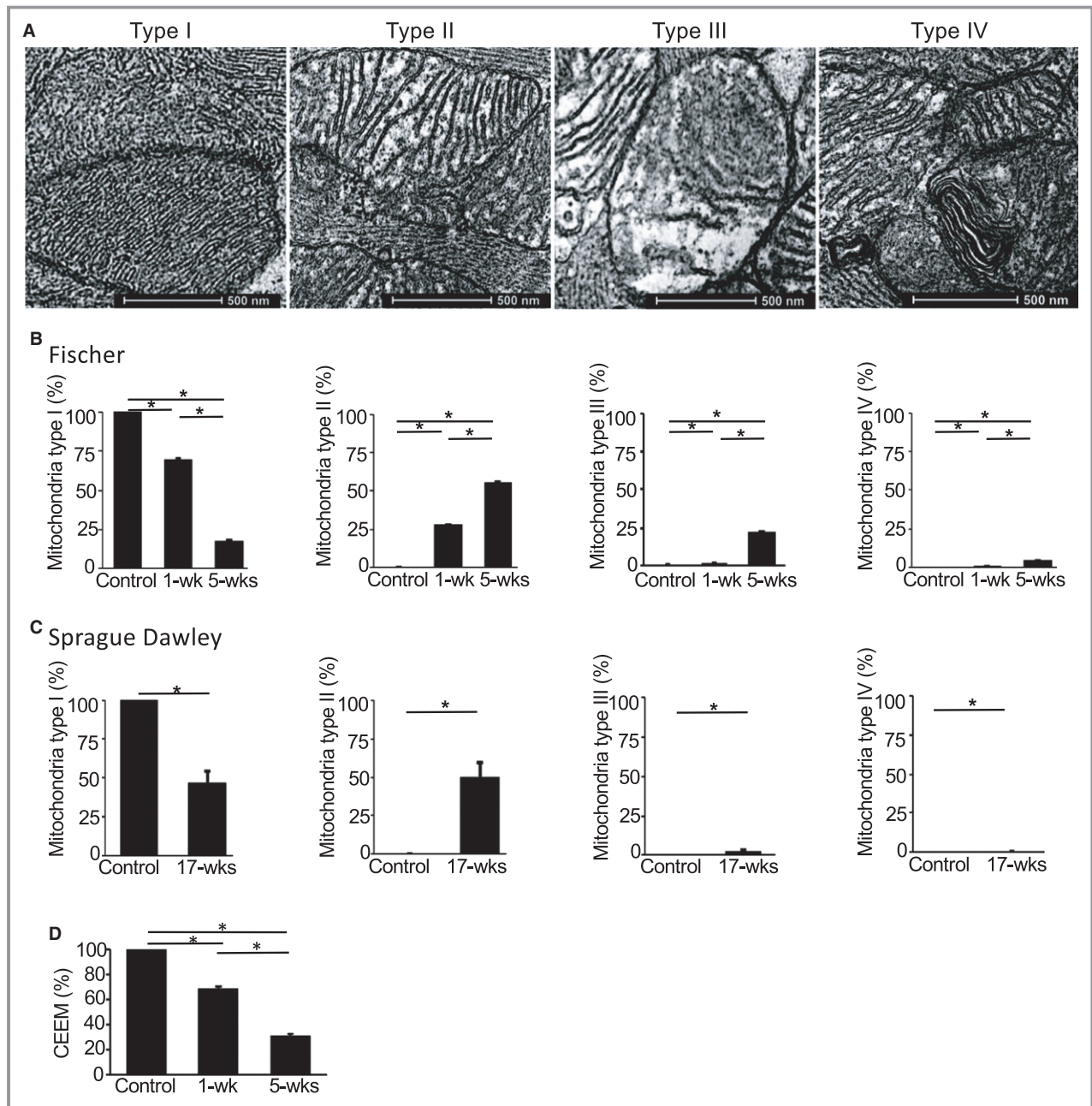
Figure 7. TEM analysis of mitochondrial types and coefficient of energy efficiency of mitochondria (CEEM) in the RV of rats with PAH. **A**, Type I: Normal-appearing mitochondria with longitudinally oriented and tightly packed cristae. Type II: Abnormal mitochondria with nondistinct shape and/or nonuniform size. The cristae are swollen, irregular, or whirling, which lost a longitudinal orientation and/or the tightness and regular spacing. Type III: The shapes and sizes of mitochondria are quite varied with the discontinuous outer membrane, cristae homogenization and fragmentation, with swollen and electron lucent matrix. Type IV: The mitochondria with the disrupted outer membrane, deficient in cristae, and myelin-like transformation. Magnification ×45 000. **B**, Means±SEM of % of mitochondrial types (I-IV) in Fischer rats with PAH at 1 and 5 weeks after the initiation of SU5416/hypoxia treatment. **C**, Means±SEM of % of mitochondrial types (I-IV) in SD rats with PAH at 17 weeks after the initiation of SU5416/hypoxia treatment. **D**, Means±SEM of % of CEEM in control and PAH Fischer rats (1- and 5-week time points). *Significantly different from each other at $P<0.05$. CEEM indicates coefficient of energy efficiency of mitochondria; PAH, pulmonary arterial hypertension; RV, right ventricle; SD, Sprague–Dawley rats; TEM, transmission electron tomography.

laboratory, the results were more consistent with >90% of rats dying between 5 and 6 weeks. In these rats, our rigorous pathological examinations defined that the cause of death was indeed congestive heart failure. Thus, Fischer (CDF) rats treated with SU5416/hypoxia represent an invaluable model that simulates human PAH-induced heart failure and death.

Compared with SU5416/hypoxia-treated SD rats we have extensively studied in the past,[13,15,18,19,21] Fischer rats treated with the same SU5416/hypoxia procedure seem to develop pulmonary vascular and RV remodeling faster. However, the degree of RV pressure elevation and extent of RV fibrosis that occur at the peak of RV damage seem to be comparable. Thus, these rat strains represent 2 distinct situations in which SD rats are capable of adapting and repairing RV damage,[18,19] while Fischer rats seem to lack such mechanisms. Understanding the differences between the RVs of these 2 rat strains should provide critical knowledge that may help treat RV failure in the setting of PAH.

TEM demonstrated progressive changes in cytoarchitectonic structures after the SU5416/hypoxia treatment of Fischer rats. These ultrastructural alterations were generally characterized by the alterations of myofilaments, the T-tubule/SR and mitochondria, all of which would have significant consequences on performing contractile functions. While the reduction in myofibrils was found to be minimal, their disorganization can suppress muscle contraction. We noted an ≈50% reduction in T-tubule/SR volume, indicating that Ca^{2+}-induced Ca^{2+} release is likely to decrease in the RV of PAH rats. These changes in the contractile and Ca^{2+} regulatory system may have contributed to the occurrence of RV failure.

The disruption of mitochondrial structure should reflect the inhibition of oxidative phosphorylation and the formation of ATP. The CEEM estimates that the mitochondrial energy production at 1 week after the SU5416 injection reduced by 30%, indicating that despite an increase in the number and volume density of mitochondria at this time point, energy production by the mitochondria is inadequate to accommodate the hypertrophied myofibrils and increased myocardial energy demand. The CEEM was dramatically reduced by 68% at 5 weeks after the SU5416 injection. Similarly, RVs of these Fischer rats with PAH exhibited Type III and IV mitochondria that are indicative of damaged mitochondria. By contrast, such mitochondrial alterations were not observed in SD rats. Thus, a deficit in mitochondrial energy production appears to be an important determinant of PAH-induced congestive heart failure as seen in Fischer rats.

These results are consistent with reports from other animal models of PAH and in human RV failure that the metabolic shift from oxidative mitochondrial metabolism to glycolytic metabolism occurs in the RV myocardium.[31] Archer and co-workers have reported that the mitochondrial density is decreased and the mitochondrial structures are changed in the monocrotaline model of PAH, and proposed the importance of mitochondria fission in RV failure.[32] Our TEM data substantiate these findings by showing the increased number of mitochondria and increased IMJ as indications of the occurrence of mitochondria fission in the Fischer rat model of PAH. Interestingly, recent transcriptomic studies in monocrotaline-treated rats also revealed that the mitochondrial pathway is most affected in RV failure.[33] By contrast, in our SD rats treated with SU5416/hypoxia that do not die of heart failure, no indications of the mitochondria fission were observed, despite the occurrence of substantial cardiac fibrosis. Thus, the preservation of mitochondria biology seems to be integral for the damaged RV to survive.

Similarly to the previously reported studies of human patients,[34] the microvessel density in the RV of Fischer rats with PAH was found to be significantly lower than that in control rats. These results suggest that the microcirculation density may also be another important determinant of the RV damage and right heart failure.

PAH has been recognized as a systemic disease and skeletal muscles have been shown to be affected in human PAH.[35] Consistent with this idea, the present study demonstrated that Fischer rats with PAH possess dramatically distorted skeletal muscle ultrastructure. Thus, this model may be useful for further investigations of the systemic nature of PAH.

In summary, in contrast to the widely used SD rat stain, the treatment of the Fischer rat strain with SU5416/hypoxia results in congestive heart failure–induced death, similar to the situation in human patients. The SU5416/hypoxia model of Fischer rats should be useful for investigating the mechanism of RV failure and finding effective therapeutic agents to increase the survival of PAH patients.

Sources of Funding

Disclosures

None.

References

1. Fallah F. Recent strategies in treatment of pulmonary arterial hypertension, a review. *Glob J Health Sci*. 2015;7:307–322.

2. Rosenkranz S. Pulmonary hypertension 2015: current definitions, terminology, and novel treatment options. *Clin Res Cardiol*. 2015;104:197–207.

3. Delcroix M, Naeije R. Optimising the management of pulmonary arterial hypertension patients: emergency treatments. *Eur Respir Rev*. 2010;19:204–211.

4. McLaughlin VV, Shah SJ, Souza R, Humbert M. Management of pulmonary arterial hypertension. *J Am Coll Cardiol*. 2015;65:1976–1997.

5. D'Alonzo GE, Barst RJ, Ayres SM, Bergofsky EH, Brundage BH, Detre KM, Fishman AP, Goldring RM, Groves BM, Kernis JT, Levy PS, Pietra GG, Reid LM, Reeves JT, Rich S, Vreim CE, Williams GW, Wu M. Survival in patients with primary pulmonary hypertension. Results from a national prospective registry. *Ann Intern Med*. 1991;115:343–349.

6. Runo JR, Loyd JE. Primary pulmonary hypertension. *Lancet*. 2003;361:1533–1544.

7. Benza RL, Miller DP, Frost A, Barst RJ, Krichman AM, McGoon MD. Analysis of the lung allocation score estimation of risk of death in patients with pulmonary arterial hypertension using data from the REVEAL Registry. *Transplantation*. 2010;90:298–305.

8. Humbert M, Sitbon O, Yaïci A, Montani D, O'Callaghan DS, Jaïs X, Parent F, Savale L, Natali D, Günther S, Chaouat A, Chabot F, Cordier JF, Habib G, Gressin V, Jing ZC, Souza R, Simonneau G; French Pulmonary Arterial Hypertension Network. Survival in incident and prevalent cohorts of patients with pulmonary arterial hypertension. *Eur Respir J*. 2010;36:549–555.

9. Thenappan T, Shah SJ, Rich S, Tian L, Archer SL, Gomberg-Maitland M. Survival in pulmonary arterial hypertension: a reappraisal of the NIH risk stratification equation. *Eur Respir J*. 2010;35:1079–1087.

10. Olsson KM, Delcroix M, Ghofrani HA, Tiede H, Huscher D, Speich R, Grünig E, Staehler G, Rosenkranz S, Halank M, Held M, Lange TJ, Behr J, Klose H, Claussen M, Ewert R, Opitz CF, Vizza CD, Scelsi L, Vonk-Noordegraaf A, Kaemmerer H, Gibbs JS, Coghlan G, Pepke-Zaba J, Schulz U, Gorenflo M, Pittrow D, Hoeper MM. Anticoagulation and survival in pulmonary arterial hypertension: results from the Comparative, Prospective Registry of Newly Initiated Therapies for Pulmonary Hypertension (COMPERA). *Circulation*. 2014;129:57–65.

11. Taraseviciene-Stewart L, Kasahara Y, Alger L, Hirth P, Mc Mahon G, Waltenberger J, Voelkel NF, Tuder RM. Inhibition of the VEGF receptor 2 combined with chronic hypoxia causes cell death-dependent pulmonary endothelial cell proliferation and severe pulmonary hypertension. *FASEB J*. 2001;15:427–438.

12. Oka M, Homma N, Taraseviciene-Stewart L, Morris KG, Kraskauskas D, Burns N, Voelkel NF, McMurtry IF. Rho kinase-mediated vasoconstriction is important in severe occlusive pulmonary arterial hypertension in rats. *Circ Res*. 2007;100:923–929.

13. Ibrahim YF, Wong CM, Pavlickova L, Liu L, Trasar L, Bansal G, Suzuki YJ. Mechanism of the susceptibility of remodeled pulmonary vessels to drug-induced cell killing. *J Am Heart Assoc*. 2014;3:e000520. DOI: 10.1161/JAHA.113.000520.

14. Alzoubi A, Toba M, Abe K, O'Neill KD, Rocic P, Fagan KA, McMurtry IF, Oka M. Dehydroepiandrosterone restores right ventricular structure and function in rats with severe pulmonary arterial hypertension. *Am J Physiol Heart Circ Physiol*. 2013;304:H1708–H1718.

15. Wang X, Ibrahim YF, Das D, Zungu-Edmondson M, Shults NV, Suzuki YJ. Carfilzomib reverses pulmonary arterial hypertension. *Cardiovasc Res*. 2016;110:188–199.

16. Bogaard HJ, Natarajan R, Henderson SC, Long CS, Kraskauskas D, Smithson L, Ockaili R, McCord JM, Voelkel NF. Chronic pulmonary artery pressure elevation is insufficient to explain right heart failure. *Circulation*. 2009;120:1951–1960.

17. Bogaard HJ, Natarajan R, Mizuno S, Abbate A, Chang PJ, Chau VQ, Hoke NN, Kraskauskas D, Kasper M, Salloum FN, Voelkel NF. Adrenergic receptor blockade reverses right heart remodeling and dysfunction in pulmonary hypertensive rats. *Am J Respir Crit Care Med*. 2010;182:652–660.

18. Zungu-Edmondson M, Shults NV, Wong CM, Suzuki YJ. Modulators of right ventricular apoptosis and contractility in a rat model of pulmonary hypertension. *Cardiovasc Res*. 2016;110:30–39.

19. Zungu-Edmondson M, Shults NV, Melnyk O, Suzuki YJ. Natural reversal of pulmonary vascular remodeling and right ventricular remodeling in SU5416/hypoxia-treated Sprague-Dawley rats. *PLoS One*. 2017;12:e0182551.

20. Jiang B, Deng Y, Suen C, Taha M, Chaudhary KR, Courtman DW, Stewart DJ. Marked strain-specific differences in the SU5416 rat model of severe pulmonary arterial hypertension. *Am J Respir Cell Mol Biol*. 2016;54:461–468.

21. Ibrahim YF, Shults NV, Rybka V, Suzuki YJ. Docetaxel reverses pulmonary vascular remodeling by decreasing autophagy and resolves right ventricular fibrosis. *J Pharmacol Exp Ther*. 2017;363:20–34.

22. Schmiedl A, Schnabel PA, Mall G, Gebhard MM, Hunneman DH, Richter J, Bretschneider HJ. The surface to volume ratio of mitochondria, a suitable parameter for evaluating mitochondrial swelling. Correlations during the course of myocardial global ischaemia. *Virchows Arch A Pathol Anat Histopathol*. 1990;416:305–315.

23. Rakusan K, Tomanek RJ. Distribution of mitochondria in normal and hypertrophic myocytes from the rat heart. *J Mol Cell Cardiol*. 1986;18:299–305.

24. Mendez J, Keys A. Density and composition of mammalian muscle. *Metabolism*. 1961;9:184–188.

25. Weibel ER, Kistler GS, Scherle WF. Practical stereological methods for morphometric cytology. *J Cell Biol*. 1966;30:23–38.

26. Paukov VS, Kazanskaya TA, Frolov VA. Quantitative analysis of some components of myocardial electron micrographs. *Bull Exp Biol Med*. 1971;71:469–472.

27. Wang X, Shults NV, Suzuki YJ. Oxidative profiling of the failing right heart in rats with pulmonary hypertension. *PLoS One*. 2017;12:e0176887.

28. Goel MK, Khanna P, Kishore J. Understanding survival analysis: Kaplan-Meier estimate. *Int J Ayurveda Res*. 2010;1:274–278.

29. Picard M, McManus MJ, Csordás G, Várnai P, Dorn GW II, Williams D, Hajnóczky G, Wallace DC. Trans-mitochondrial coordination of cristae at regulated membrane junctions. *Nat Commun*. 2015;6:6259.

30. Mannella CA, Lederer WJ, Jafric MS. The connection between inner membrane topology and mitochondrial function. *J Mol Cell Cardiol*. 2013;62:51–57.

31. Piao L, Marsboom G, Archer SL. Mitochondrial metabolic adaptation in right ventricular hypertrophy and failure. *J Mol Med (Berl)*. 2010;88:1011–1020.

32. Tian L, Neuber-Hess M, Mewburn J, Dasgupta A, Dunham-Snary K, Wu D, Chen KH, Hong Z, Sharp WW, Kutty S, Archer SL. Ischemia-induced Drp1 and Fis1-mediated mitochondrial fission and right ventricular dysfunction in pulmonary hypertension. *J Mol Med (Berl)*. 2017;95:381–393.

33. Potus F, Hindmarch CCT, Dunham-Snary KJ, Stafford J, Archer SL. Transcriptomic signature of right ventricular failure in experimental pulmonary arterial hypertension: deep sequencing demonstrates mitochondrial, fibrotic, inflammatory and angiogenic abnormalities. *Int J Mol Sci*. 2018;19:E2730.

34. Potus F, Ruffenach G, Dahou A, Thebault C, Breuils-Bonnet S, Tremblay È, Nadeau V, Paradis R, Graydon C, Wong R, Johnson I, Paulin R, Lajoie AC, Perron J, Charbonneau E, Joubert P, Pibarot P, Michelakis ED, Provencher S, Bonnet S. Downregulation of microRNA-126 contributes to the failing right ventricle in pulmonary arterial hypertension. *Circulation*. 2015;132:932–943.

35. Malenfant S, Potus F, Fournier F, Breuils-Bonnet S, Pflieger A, Bourassa S, Tremblay È, Nehmé B, Droit A, Bonnet S, Provencher S. Skeletal muscle proteomic signature and metabolic impairment in pulmonary hypertension. *J Mol Med (Berl)*. 2015;93:573–584.